

Real-time diagrammatic approach to transport through interacting quantum dots with normal and superconducting leads

Michele Governale¹, Marco G. Pala², and Jürgen König^{1,3}

¹*Institut für Theoretische Physik III, Ruhr-Universität Bochum, 44780 Bochum, Germany*

²*IMEP-LAHC-MINATEC (UMR CNRS/INPG/UJF 5130), 38016 Grenoble, France*

³*Theoretische Physik, Universität Duisburg-Essen, 47048 Duisburg, Germany*

(Dated: November 7, 2018)

We present a real-time diagrammatic theory for transport through interacting quantum dots tunnel coupled to normal and superconducting leads. Our formulation describes both the equilibrium and non-equilibrium superconducting proximity effect in a quantum dot. We study a three-terminal transistor geometry, consisting of a single-level quantum dot tunnel coupled to two phase-biased superconducting leads and one voltage-biased normal lead. We compute both the Josephson current between the two superconductors and the Andreev current in the normal lead, and analyze their switching on and off as well as transitions between 0- and π -states as a function of gate and bias voltage. For the limit of large superconducting gaps in the leads, we describe the formation of Andreev bound states within an exact resummation of all orders in the tunnel coupling to the superconducting leads, and discuss their signature in the non-equilibrium Josephson- and Andreev-current and the quantum-dot charge.

PACS numbers: 74.45.+c, 73.23.Hk, 73.63.Kv, 73.21.La

I. INTRODUCTION

Continuous advancements in nanofabrication have made it possible to attach superconducting leads to quantum dots. The supercurrent through a quantum dot has been measured through dots realized in carbon nanotubes¹ and in InAs nanowires.² Recently, transport measurements on a single self-assembled InAs quantum dot coupled to Al superconducting electrodes have been reported.³

From a theoretical point of view, quantum dots coupled to superconducting leads are of great interest, since a very rich physics is expected from the combination of superconducting correlations, electron-electron interaction and non-equilibrium in the dot. Subgap transport through a normal-dot-superconductor system is sustained by Andreev reflection.^{4,5,6,7,8,9} The Josephson coupling between two superconductors through a quantum dot has been addressed in the limit of a non-interacting quantum dot in Ref. 10. In the opposite limit of a large charging energy, the electrons forming a Cooper pair tunnel one by one via virtual dot states,^{11,12,13} which establishes a Josephson current carried by higher-order tunneling processes. Other aspects of the problem, such as the Kondo regime^{11,14,15,16,17,18,19,20} or multiple Andreev reflection^{21,22} have also been addressed. The dependence of the charge in the quantum dot on the gate voltage and on the superconducting phase difference has been investigated in Ref. 23. Moreover, numerical approaches based on the non-crossing approximation,²⁴ the numerical renormalization group²⁵ and Monte Carlo²⁶ have been employed to study transport through this type of systems. The authors of Ref. 27 compare different approximation schemes, such as mean field and second-order perturbation in the Coulomb interaction. The proximity effect in double-dot systems has been also in-

vestigated in different regimes.^{17,18,28} In Ref. 29 the non-equilibrium Josephson and Andreev currents through a dot coupled to one normal and two superconducting leads have been studied in the weak-proximity limit, considering only first-order processes in the tunnel coupling with the superconductors. In this regime, finite Josephson and Andreev currents can flow only if the dot is driven out of equilibrium. The idea of using non-equilibrium to control the behavior of a Josephson junction has been proposed³⁰ and experimentally tested³¹ some years ago.

In the present work, we develop a real-time transport theory for an interacting quantum dot connected to both superconducting and normal leads. The theory can be conveniently formulated by means of a diagrammatic language and it is suitable for dealing with superconducting correlations, strong Coulomb interaction and non-equilibrium due to arbitrary bias voltages on the same footing. We demonstrate the use of our formalism for two examples. First, we study the equilibrium Josephson current between two superconductors due to cotunneling through the quantum dot and analyze the formation of a π -state for increasing on-site Coulomb repulsion on the dot. Second, we consider a transistor geometry with one normal and two superconducting leads with large superconducting gaps. We calculate the non-equilibrium Josephson and Andreev current to all orders in the coupling strength with the superconductors, where the quantum dot is driven out of equilibrium by applying a bias voltage to the normal lead. This geometry is suitable for performing a spectroscopy of the Andreev bound states in the interacting quantum dot.

II. MODEL AND FORMALISM

A. Hamiltonian

We consider a single-level quantum dot tunnel coupled to both normal and superconducting leads. The total Hamiltonian of the system is given by

$$H = H_D + \sum_{\eta} (H_{\eta} + H_{\text{tunn},\eta}). \quad (1)$$

The different (superconducting or normal) leads are labeled by the index η . The quantum dot is described by the Hamiltonian of the single-level Anderson model,

$$H_D = \sum_{\sigma} \epsilon d_{\sigma}^{\dagger} d_{\sigma} + U n_{\uparrow} n_{\downarrow}, \quad (2)$$

where d_{σ} (d_{σ}^{\dagger}) is the annihilation (creation) operator for an electron in the dot, ϵ denotes the energy of the single-particle level, $n_{\sigma} = d_{\sigma}^{\dagger} d_{\sigma}$ is the number operator for spin $\sigma = \uparrow, \downarrow$, and U is the energy cost for double occupation. The leads' electrons are described by the annihilation and creation operators $c_{\eta k \sigma}$ and $c_{\eta k \sigma}^{\dagger}$, respectively. In addition to the kinetic-energy term $\sum_{k \sigma} \epsilon_k c_{\eta k \sigma}^{\dagger} c_{\eta k \sigma}$ in the Hamiltonian, there may be a BCS pair-interaction part $-g_{\eta} \sum_{k, k'} c_{\eta k \uparrow}^{\dagger} c_{\eta -k \downarrow}^{\dagger} c_{\eta -k' \downarrow} c_{\eta k' \uparrow}$ to account for superconductivity. On the one hand, we want to treat the interaction on a mean-field level. On the other hand, we want to keep track of the total number of electrons, which will be important for situations with finite bias voltage between different superconductors. This can be achieved by representing the lead electrons in terms of Bogoliubov quasiparticle operators $\gamma_{\eta k \sigma}^{(\dagger)}$ and Cooper-pair annihilation (creation) operators³² $S_{\eta}^{(\dagger)}$ via the Bogoliubov transform

$$\begin{pmatrix} \gamma_{\eta k \uparrow} \\ \gamma_{\eta -k \downarrow}^{\dagger} \end{pmatrix} = \begin{pmatrix} u_{\eta k} & -v_{\eta k} S_{\eta} \\ v_{\eta k}^* S_{\eta}^{\dagger} & u_{\eta k}^* \end{pmatrix} \begin{pmatrix} c_{\eta k \uparrow} \\ c_{\eta -k \downarrow}^{\dagger} \end{pmatrix}. \quad (3)$$

with coefficients

$$u_k = \sqrt{\frac{1}{2} \left(1 + \frac{\epsilon_k - \mu_{\eta}}{\sqrt{(\epsilon_k - \mu_{\eta})^2 + |\Delta_{\eta}|^2}} \right)} \quad (4)$$

$$v_k = e^{i\Phi_{\eta}} \sqrt{\frac{1}{2} \left(1 - \frac{\epsilon_k - \mu_{\eta}}{\sqrt{(\epsilon_k - \mu_{\eta})^2 + |\Delta_{\eta}|^2}} \right)}, \quad (5)$$

where μ_{η} is the electrochemical potential of lead η and Φ_{η} the phase of the order parameter $\Delta_{\eta} \equiv g_{\eta} \sum_k \langle S_{\eta}^{\dagger} c_{\eta -k \downarrow} c_{\eta k \uparrow} \rangle$. As a result, the mean-field Hamiltonian for lead η reads

$$H_{\eta} = \sum_{k \sigma} E_{\eta k} \gamma_{\eta k \sigma}^{\dagger} \gamma_{\eta k \sigma} + \mu_{\eta} N, \quad (6)$$

plus an irrelevant constant. Here, $E_{\eta k} = \sqrt{(\epsilon_k - \mu_{\eta})^2 + |\Delta_{\eta}|^2}$ is the quasiparticle energy, and

N is the total number of electrons, which equals the number of Bogoliubov quasiparticles plus twice the number of Cooper pairs. In the case that η refers to a normal lead, the order parameter vanishes, $\Delta_{\eta} = 0$.

The coupling between the dot and the leads is taken into account by the tunneling Hamiltonians

$$H_{\text{tunn},\eta} = V_{\eta} \sum_{k \sigma} \left(c_{\eta k \sigma}^{\dagger} d_{\sigma} + \text{H.c.} \right), \quad (7)$$

where for the sake of simplicity the tunnel matrix elements V_{η} are considered to be spin and wavevector independent. The tunnel-coupling strengths are defined as $\Gamma_{\eta} = 2\pi |V_{\eta}|^2 \sum_k \delta(\omega - \epsilon_k)$, which we assume to be energy independent.

B. Diagrammatic Real-Time Technique

The main idea of the diagrammatic real-time technique is to integrate out all the (noninteracting) fermionic degrees of freedom in the leads to arrive at an effective description for the reduced system, that is characterized by the state of the quantum dot and the number of Cooper pairs in the superconducting leads. The Hilbert space of the single-level quantum dot is four dimensional: the dot can be empty, singly occupied with a spin-up or spin-down electron, or doubly occupied. These are denoted by $|\chi\rangle \in \{|0\rangle, |\uparrow\rangle, |\downarrow\rangle, |D\rangle \equiv d_{\uparrow}^{\dagger} d_{\downarrow}^{\dagger} |0\rangle\}$, and have energies E_0 , $E_{\uparrow} = E_{\downarrow}$, and E_D , respectively. The condensates in the superconducting leads are characterized by the number of Cooper pairs $|\mathbf{n}\rangle$, relative to some arbitrarily chosen reference, where \mathbf{n} is the vector of Cooper-pair numbers n_{η} for each superconducting lead η . The energy contribution from the Cooper-pair condensates is given by $E_{\mathbf{n}} = \sum_{\eta} 2n_{\eta} \mu_{\eta}$. If all superconducting leads are kept at the same chemical potential then this energy contribution simply provides a trivial additive constant. For finite bias voltage between at least two superconducting leads, however, the total energy depends on how the Cooper pairs are distributed among the superconducting leads.

We start with the full density matrix of the total system, including the quantum dot, the fermionic degrees of freedom of the leads, and the Cooper-pair condensates. Since the fermionic degrees of freedom in the leads act as reservoirs, we can trace them out to obtain the reduced density matrix ρ_{red} with matrix elements $P_{\xi_2}^{\xi_1} \equiv \langle \xi_1 | \rho_{\text{red}} | \xi_2 \rangle$.

Here, the label $\xi \equiv (\chi, \mathbf{n})$ with energy $E_{\xi} = E_{\chi} + E_{\mathbf{n}}$ includes both the quantum-dot state χ and the number of Cooper pairs, \mathbf{n} , in the leads. For the diagonal elements of the reduced density matrix we also use the notation $P_{\xi} \equiv P_{\xi}^{\xi}$.

1. Kinetic equation and current formula

The dynamics of the reduced density matrix is governed by the kinetic or generalized master equation,

$$\frac{d}{dt}P_{\xi_2}^{\xi_1}(t) + \frac{i}{\hbar}(E_{\xi_1} - E_{\xi_2})P_{\xi_2}^{\xi_1}(t) = \sum_{\xi_1'\xi_2'} \int_{-\infty}^t dt' W_{\xi_2\xi_2'}^{\xi_1\xi_1'}(t, t')P_{\xi_2'}^{\xi_1'}(t'), \quad (8)$$

where the kernels $W_{\xi_2\xi_2'}^{\xi_1\xi_1'}(t, t')$ describe transitions due to tunneling. The current in lead η can be written as

$$J_\eta(t) = -e \sum_{\xi_1'\xi_2'} \int_{-\infty}^t dt' W_{\xi_2\xi_2'}^{\xi_1\xi_1'\eta}(t, t')P_{\xi_2'}^{\xi_1'}(t'), \quad (9)$$

where $W_{\xi_2\xi_2'}^{\xi_1\xi_1'\eta}(t, t') \equiv \sum_s s W_{\xi_2\xi_2'}^{\xi_1\xi_1's\eta}(t, t')$, and $W_{\xi_2\xi_2'}^{\xi_1\xi_1's\eta}(t, t')$ is the sum of all kernels that describe transitions in which in total s electrons are removed from lead η .

Both the generalized master equation and the expression for the current can be further simplified when all voltages and coupling strengths are kept time independent. The kernels do, then, only depend on the time difference $t - t'$, and to determine the DC component of the current and all density matrix elements we only need the time integrals of the kernels, which we refer to as generalized rates $W_{\xi_2\xi_2'}^{\xi_1\xi_1'}/\hbar \equiv \int_{-\infty}^t dt' W_{\xi_2\xi_2'}^{\xi_1\xi_1'}(t - t')$ and generalized current rates $W_{\xi_2\xi_2'}^{\xi_1\xi_1'\eta}/\hbar \equiv \int_{-\infty}^t dt' W_{\xi_2\xi_2'}^{\xi_1\xi_1'\eta}(t - t')$.

The indices ξ contain more information than needed for our purpose. This is related to the fact that only the change and not the absolute value of the number of Cooper pairs in each superconducting lead matters, i.e. the value of the generalized rate $W_{\xi_2\xi_2'}^{\xi_1\xi_1'}$ does not change when we perform the simultaneous shift $\mathbf{n}_1 \rightarrow \mathbf{n}_1 + \mathbf{m}$, $\mathbf{n}_2 \rightarrow \mathbf{n}_2 + \mathbf{m}$, $\mathbf{n}'_1 \rightarrow \mathbf{n}'_1 + \mathbf{m}$, and $\mathbf{n}'_2 \rightarrow \mathbf{n}'_2 + \mathbf{m}$ for a given vector of additional Cooper-pair numbers \mathbf{m} . After defining

$$P_{\chi_2}^{\chi_1}(\mathbf{m}) \equiv \sum_{\mathbf{n}} P_{(\chi_2, \mathbf{n})}^{(\chi_1, \mathbf{m} + \mathbf{n})} \quad (10)$$

$$W_{\chi_2\chi_2'}^{\chi_1\chi_1'}(\mathbf{m}, \mathbf{m}') \equiv \sum_{\mathbf{n}, \mathbf{n}'} W_{(\chi_2, \mathbf{n})(\chi_2', \mathbf{n}')}^{(\chi_1, \mathbf{m} + \mathbf{n})(\chi_1', \mathbf{m}' + \mathbf{n}')}, \quad (11)$$

and similarly for the generalized current rates, we obtain for the stationary current in lead η

$$J_\eta = -\frac{e}{\hbar} \sum_{\chi\chi'} W_{\chi\chi'}^{\chi\chi'\eta}(\mathbf{0}, \mathbf{n}')P_{\chi'}^{\chi}(\mathbf{n}'), \quad (12)$$

where the matrix elements $P_{\chi'}^{\chi}(\mathbf{n}')$ are determined from

$$i(E_{\chi_1} - E_{\chi_2} + E_{\mathbf{n}})P_{\chi_2}^{\chi_1}(\mathbf{n}) = \sum_{\chi_1'\chi_2'\mathbf{n}'} W_{\chi_2\chi_2'}^{\chi_1\chi_1'}(\mathbf{n}, \mathbf{n}')P_{\chi_2'}^{\chi_1'}(\mathbf{n}') \quad (13)$$

together with the normalization condition $\sum_{\chi} P_{\chi}^{\chi}(\mathbf{0}) = 1$. Note that, in Eqs. (12) and (13), due to conservation of the total number of electrons, only those Cooper-pair-number vectors \mathbf{n} appear for which $\sum_{\eta} n_{\eta}$ equals twice the number of dot electrons in state χ_2 minus that in state χ_1 (and the same holds true for \mathbf{n}' , χ_2' , and χ_1'). The generalized master equations for $P_{\chi_2}^{\chi_1}(\mathbf{n})$ with all other vectors \mathbf{n} , not satisfying the condition stated above, decouple and are, therefore, irrelevant. For illustration, let us consider the matrix element $P_{\mathbf{0}}^{\mathbf{D}}(\mathbf{n})$ in a system with two superconducting leads; for example, with $\mathbf{n} = (-1, 0)$ or $\mathbf{n} = (-2, 1)$ it contributes, while with $\mathbf{n} = (1, 0)$ it is irrelevant.

In the special case that all superconducting leads are at the same chemical potential μ_S , the situation simplifies further. Due to the fact that in Eq. (13) the energy contribution $E_{\mathbf{n}}$ is the same for all \mathbf{n} that are compatible with χ_1 and χ_2 , the generalized master equation Eq. (13) remains unchanged under the shift $\mathbf{n} \rightarrow \mathbf{n} + \mathbf{m}$ and $\mathbf{n}' \rightarrow \mathbf{n}' + \mathbf{m}$ with $\sum_{\eta} m_{\eta} = 0$. As a consequence, the generalized rates $W_{\chi_2\chi_2'}^{\chi_1\chi_1'}$ and $W_{\chi\chi'}^{\chi\chi'\eta}$ as well as the solution for $P_{\chi_2}^{\chi_1}$ become independent of the Cooper-pair numbers, i.e., we can simply drop the arguments $\mathbf{0}$, \mathbf{n} and \mathbf{n}' . It is this limit that we are going to analyze in the results section of this paper.

2. Time evolution of the reduced density matrix

We generalize the real-time diagrammatic approach to transport through interacting quantum dots of Ref. 34 to the case of superconducting leads. Our goal is to give a diagrammatic prescription to compute the generalized rates $W_{\chi_2\chi_2'}^{\chi_1\chi_1'}(\mathbf{n}, \mathbf{n}')$ and $W_{\chi\chi'}^{\chi\chi'\eta}(\mathbf{0}, \mathbf{n}')$. For this, we analyze the time evolution of the reduced density matrix that we obtain by integrating out the fermionic degrees of freedom in the leads.

We assume at some initial time t_0 (with $t_0 \rightarrow -\infty$) the total system to be in a product state of the leads' fermionic degrees of freedom (taken at equilibrium) and the degrees of freedom of the reduced system. The time evolution of the reduced density matrix from time t_0 to time t can, then, be described by $P_{\xi_2}^{\xi_1}(t) = \sum_{\xi_1'\xi_2'} \Pi_{\xi_2\xi_2'}^{\xi_1\xi_1'}(t, t_0)P_{\xi_2'}^{\xi_1'}(t_0)$. The propagator $\Pi_{\xi_2\xi_2'}^{\xi_1\xi_1'}(t, t_0)$ can be computed by means of a perturbation expansion in the tunneling Hamiltonian $H_{\text{tunn}} = \sum_{\eta} H_{\text{tunn},\eta}$. How this is done has been explained elsewhere³⁴ and here we will limit ourselves to sketch briefly the derivation, thereby pointing out the new ingredients due to superconductivity. The propagator (starting from and ending at a product state of the leads' fermions and the reduced system) is written in interaction representation with respect to H_{tunn} as

$$\Pi_{\xi_2 \xi_2'}^{\xi_1 \xi_1'}(t, t') = \text{Tr}_{\text{leads}} \left\{ \langle \xi_2'(t') | T_K \left[|\xi_2(t)\rangle \langle \xi_1(t) | e^{-\frac{i}{\hbar} \int_{K_{t' \rightarrow t}} dt'' H_{\text{tunn}}(t'') } \right] | \xi_1'(t') \rangle \right\}, \quad (14)$$

being $K_{t' \rightarrow t}$ the Keldysh contour going from t' to t and then backwards to t' , T_K the time-ordering operator on the Keldysh contour, $H_{\text{tunn}}(t)_I$ the tunnel Hamiltonian in interaction representation, and Tr_{leads} the trace over the fermionic part of the lead degrees of freedom.

Next, we expand the exponential function in a power series of H_{tunn} . Finally, we perform the trace over the fermionic lead degrees of freedom by means of Wick's theorem. This is possible because the Hamiltonians of the leads are quadratic in the lead fermionic operators (this applies also to the superconductors in the mean-field description adopted here).

For normal leads, only contractions between electron creation and annihilation operators are non zero. They are graphically depicted as tunneling lines (*normal lines*) with an arrow going from the vertex $c_{\eta k \sigma}^\dagger d_\sigma$ to the vertex $d_\sigma^\dagger c_{\eta k \sigma}$. We define the direction of the line such that an electron is removed from the dot at the vertex where the line starts and added to the dot at the vertex where the line ends.

For the superconducting leads two different types of lines appear. There are again *normal lines*, connecting a vertex $c_{\eta k \sigma}^\dagger d_\sigma$ with the $d_\sigma^\dagger c_{\eta k \sigma}$. In addition, there are *anomalous lines*, connecting either $c_{\eta k \sigma}^\dagger d_\sigma$ with $c_{\eta-k-\sigma}^\dagger d_{-\sigma}$, or $d_\sigma^\dagger c_{\eta k \sigma}$ with $d_{-\sigma}^\dagger c_{\eta-k-\sigma}$. Due to the con-

vention for the arrow direction introduced above, the anomalous lines carry two arrows that point towards each other (*outgoing anomalous line*) if two annihilation operators of dot electrons are involved, and away from each other (*incoming anomalous line*) for two creation operators of dot electrons. To evaluate the contractions, it is convenient to perform the Bogoliubov transform for the lead electron operators. Since the Bogoliubov transform involves the operators $S_\eta^{(\dagger)}$, the number of Cooper pairs in lead η may be changed at the tunnel vertices. For each normal and each anomalous superconducting line, there are two possibilities. The vertices being connected by normal lines either involve no operator $S_\eta^{(\dagger)}$ or one S_η and one S_η^\dagger . For outgoing (incoming) anomalous lines, either one of the two vertices carries the operator S_η^\dagger (S_η). The normal lines describe quasiparticle tunneling. Whereas, the anomalous lines describe Andreev tunneling: for an incoming (outgoing) anomalous line a Cooper pair breaks (forms) in the lead and its constituents enter (leave) the dot at the two vertices.

Now we can describe the different contributions to the propagator by means of a graphical representation on the Keldysh contour. An example is shown in Fig. 1, where both normal and anomalous lines are present.

The propagator obeys the Dyson equation

$$\Pi_{\xi_2 \xi_2'}^{\xi_1 \xi_1'}(t, t') = \Pi_{\xi_2 \xi_2'}^{\xi_1 \xi_1(0)}(t, t') \delta_{\xi_1 \xi_1'} \delta_{\xi_2 \xi_2'} + \sum_{\xi_1'' \xi_2''} \int_{t'}^t dt'' \int_{t''}^t dt''' \Pi_{\xi_2 \xi_2}^{\xi_1 \xi_1(0)}(t, t''') W_{\xi_2 \xi_2'}^{\xi_1 \xi_1''}(t''', t'') \Pi_{\xi_2'' \xi_2'}^{\xi_1'' \xi_1'}(t'', t'), \quad (15)$$

where $\Pi_{\xi_2 \xi_2}^{\xi_1 \xi_1(0)}(t, t')$ is the free propagator and we identify $W_{\xi_2 \xi_2'}^{\xi_1 \xi_1'}(t, t')$ with the irreducible part of the propagator, i.e. with the sum of irreducible diagrams going from t' to t contributing to the propagator $\Pi_{\xi_2 \xi_2'}^{\xi_1 \xi_1'}(t, t')$, where a diagram is irreducible if any vertical line through the diagrams cuts at least one tunneling line. The order in Γ of an irreducible diagram is given by the number of tunneling lines present in the diagram. Examples of first- and second-order diagrams are shown in Fig. 1.

From now on we concentrate on stationary situations and, hence, we will consider the generalized rates. These are given by the Laplace transform of $W_{\xi_2 \xi_2'}^{\xi_1 \xi_1'}(t - t')$ computed at $z = 0^+$, i.e. $W_{\xi_2 \xi_2'}^{\xi_1 \xi_1'} = \hbar \left[\int_{-\infty}^t dt' e^{-z(t-t')} W_{\xi_2 \xi_2'}^{\xi_1 \xi_1'}(t - t') \right]_{z=0^+}$. Furthermore, we

only keep the information of Cooper-pair-number differences, i.e., we formulate the rules for $W_{\chi_2 \chi_2'}^{\chi_1 \chi_1'}(\mathbf{m}, \mathbf{m}') \equiv \sum_{\mathbf{n}, \mathbf{n}'} W_{(\chi_2, \mathbf{n})(\chi_2', \mathbf{n}')}^{(\chi_1, \mathbf{m}+\mathbf{n})(\chi_1', \mathbf{m}'+\mathbf{n}')}$. The last step does not only reduce the number of matrix elements to be considered. Another virtue is the possibility to combine different contributions. As mentioned above, for a given superconducting line there are always two possibilities to assign operators $S_\eta^{(\dagger)}$ to the two vertices. Depending on the topology of the reduced diagram, the corresponding terms may contribute to *different* generalized rates $W_{\xi_2 \xi_2'}^{\xi_1 \xi_1'}$ (that differ from each other by the number of Cooper pairs) but they always contribute to the *same* $W_{\chi_2 \chi_2'}^{\chi_1 \chi_1'}(\mathbf{m}, \mathbf{m}')$. It turns out that, since the tunneling strengths Γ_η are independent of energy, the analytic ex-

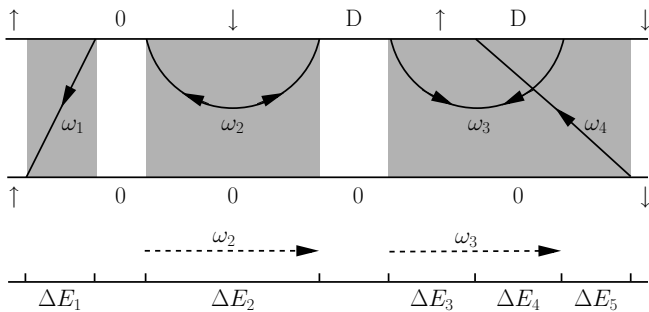


FIG. 1: Graphic representation of a contribution to the element $\Pi_{\downarrow\uparrow}^{\downarrow\uparrow}$ of the propagator for the reduced density matrix, for the exemplary case of one superconductor with chemical potential μ_S . The upper and the lower line of the Keldysh contour represents the forward and the backward propagation, respectively. From left to the right we can identify a first-order diagram with a normal line, a first-order diagram with an anomalous line, a second-order diagram with a normal and an anomalous lines. Below the diagrammatic representation of the propagator, we show our arbitrary choice for the directions of the tunneling lines and the corresponding energy differences to be used in rule 2, which are given by $\Delta E_1 = \omega_1 - \epsilon$; $\Delta E_2 = -\omega_2 - \epsilon + 2\mu_S$; $\Delta E_3 = -\omega_3 - \epsilon + 2\mu_S$; $\Delta E_4 = \omega_4 - \omega_3 - 2\epsilon - U + 2\mu_S$; $\Delta E_5 = \omega_4 - \epsilon$.

pressions of the two contributions always combine nicely, which leads to a rather compact formulation of the diagrammatic rules presented below.

As defined above, the arrows of a tunneling line indicate whether an electron enters or leaves the dot at a given tunnel vertex. Furthermore, we want to define an overall direction of each tunneling in order to define the sign of the energy carried by the Bogoliubov quasiparticles. For normal lines, we will always choose the direction set by the single arrow. For anomalous lines (that carry two opposite arrows), we pick the direction arbitrarily, and assign the creation or annihilation of a Cooper pair to the vertex at which the line direction is opposite to the arrow.

In order to construct a systematic perturbation expansion in the tunnel coupling, both the generalized rates and the probabilities are expanded in orders of Γ , i.e. $W_{\chi_2\chi_2'}^{\chi_1\chi_1'}(\mathbf{m}, \mathbf{m}') = W_{\chi_2\chi_2'}^{\chi_1\chi_1'(1)}(\mathbf{m}, \mathbf{m}') + W_{\chi_2\chi_2'}^{\chi_1\chi_1'(2)}(\mathbf{m}, \mathbf{m}') + \mathcal{O}(\Gamma^3)$ and $P_{\chi_2}^{\chi_1}(\mathbf{m}) = P_{\chi_2}^{\chi_1(0)}(\mathbf{m}) + P_{\chi_2}^{\chi_1(1)}(\mathbf{m}) + \mathcal{O}(\Gamma^2)$, where the superscript indicates the order in Γ .

3. Diagrammatic rules

The rules for evaluating the generalized rates $W_{\chi_2\chi_2'}^{\chi_1\chi_1'}(\mathbf{m}, \mathbf{m}')$ are:

1. Draw all topologically different diagrams with fixed ordering of the vertices in the real axis. The vertices are connected in pairs by tunneling lines carrying energy ω_i . The tunneling lines can be normal

or anomalous. For each anomalous line choose the direction (forward or backward with respect to the Keldysh contour) arbitrarily.

2. For each vertical cut between two vertices assign a factor $1/(\Delta E + i\eta)$ with $\eta = 0^+$, where ΔE is the difference between the left-going and the right-going energies, including the energy of the dot states, E_χ , the tunneling lines, ω_i , and the energy difference of Cooper-pair condensates, E_n . The latter is increased (decreased) at each vertex of an outgoing (incoming) anomalous line at which the arrow is opposite to the arbitrarily chosen line direction.
3. For each tunneling line assign a factor $\frac{1}{2\pi}\Gamma_\eta D_\eta(\omega_i) f_\eta^\pm(\omega_i)$, where $f_\eta^+(\omega_i) = f_\eta(\omega_i) = [1 + \exp(\omega_i - \mu_\eta)/(k_B T)]^{-1}$ and $f_\eta^-(\omega_i) = 1 - f_\eta(\omega_i)$, and $D_\eta(\omega) = \frac{|\omega - \mu_\eta|}{\sqrt{(\omega - \mu_\eta)^2 - |\Delta_\eta|^2}} \theta(|\omega - \mu_\eta| - |\Delta_\eta|)$. The upper (lower) sign applies for lines going backward (forward) with respect to the Keldysh contour. For anomalous lines multiply an additional factor $\pm \text{sign}(\omega_i) \frac{|\Delta_\eta|}{|\omega_i|}$. Moreover, assign a factor $e^{-i\Phi_\eta}$ for an outgoing and $e^{i\Phi_\eta}$ for an incoming anomalous line. [For normal leads, only normal lines with $D_\eta(\omega_i) \equiv 1$ appear.]
4. Assign an overall prefactor $-i$. Furthermore, assign a factor -1 for each
 - a) vertex on the lower propagator;
 - b) crossing of tunneling lines;
 - c) vertex that connects the doubly occupied dot state, $|D\rangle = d_\uparrow^\dagger d_\downarrow^\dagger |0\rangle$, to spin up, $|\uparrow\rangle$;
 - d) outgoing (incoming) anomalous tunneling line in which the earlier (later) tunnel vertex with respect to the Keldysh contour involves a spin up dot electron.
 [The factors in c) and d) arise due to Fermi statistics from the order of the dot and lead operators, respectively.]
5. For each diagram, integrate over all energies ω_i . Sum over all diagrams.

The generalized current rates $W_{\chi\chi_2'}^{\chi\chi_1'}(\mathbf{0}, \mathbf{m}')$ are evaluated in the following way:

6. Multiply the value of the corresponding generalized rate $W_{\chi\chi_2'}^{\chi\chi_1'}(\mathbf{0}, \mathbf{m}')$ with a factor given by adding up the following numbers for each tunneling line that is associated with lead η :
 - a) for normal lines: 1 if the line is going from the lower to the upper, -1 if it is going from the upper to the lower propagator, and 0 otherwise;
 - b) for anomalous lines: 1 for incoming lines within the upper and outgoing lines within the lower propagator, -1 for for outgoing lines within the upper

and incoming lines within the lower propagator, and 0 otherwise.

The diagrammatic rules are formulated generally enough to account for any choice of chemical potentials of the leads, i.e., we allow for any bias voltages between any pair of leads. A variety of interesting phenomena, however, shows up already when all superconducting leads are kept at the same chemical potential (set to 0 per definition), and a nonequilibrium situation is generated only by applying voltages between the normal leads and the superconductors. It is this limit that we are going to analyze in the rest of the paper. In this case, the diagrammatic language simplifies further. As already indicated above, we simply can drop all information associated with the Cooper-pair numbers in our diagrammatic rules.

C. Green's functions

If all superconducting leads are kept at the same chemical potential, which we put to 0 per definition, we can use the simplified diagram, where the information about the Cooper pairs is ignored. Such a procedure is identical to having dropped the Cooper-pair states from the very beginning in the Hamiltonian, i.e., using the Bogoliubov transform without employing the operators $S_\eta^{(\dagger)}$. For this case, the charge current in lead η has been related to the local Green's functions of the quantum dot^{14,24,29} by using the approach of Ref. 33. Here, we report the formula of Ref. 29 which is useful for what comes in the following. For the sake of keeping the notation compact, we use the Nambu representation for the dot operators: $\phi = (d_\uparrow, d_\downarrow^\dagger)^T$.

The current flowing out of lead η is written as the sum of two contributions, $J_\eta = J_{1\eta} + J_{2\eta}$, with

$$J_{1\eta} = \frac{e}{\hbar} \int \frac{d\omega}{2\pi} \Gamma_\eta D_\eta(\omega) \text{Im} \left\{ \text{Tr} \left[\tau_3 \left(\mathbf{1} - \frac{\Delta_\eta}{\omega} \right) (2\mathbf{G}^R(\omega) f_\eta(\omega) + \mathbf{G}^<(\omega)) \right] \right\}, \quad (16)$$

$$J_{2\eta} = -\frac{e}{\hbar} \int \frac{d\omega}{2\pi} \Gamma_\eta \tilde{D}_\eta(\omega) \text{Re} \left\{ \text{Tr} \left[\tau_3 \frac{\Delta_\eta}{|\Delta_\eta|} \mathbf{G}^<(\omega) \right] \right\}, \quad (17)$$

where $\Delta_\eta = \begin{pmatrix} 0 & \Delta_\eta \\ \Delta_\eta^* & 0 \end{pmatrix}$, and $f_\eta(\omega) = [1 + \exp(\omega - \mu_\eta)/(k_B T)]^{-1}$ is the Fermi function, with μ_η being the (electro-) chemical potential of lead η ($= 0$ for the superconductors), T the temperature and k_B the Boltzmann constant. The local dot Green's functions $\mathbf{G}^R(\omega)$ and $\mathbf{G}^<(\omega)$ are matrices in Nambu space, whose components $(\mathbf{G}^<(\omega))_{m,n}$ and $(\mathbf{G}^R(\omega))_{m,n}$ are defined as the Fourier transforms of $i\langle \phi_n^\dagger(0) \phi_m(t) \rangle$ and $-i\theta(t) \langle \{ \phi_m(t), \phi_n^\dagger(0) \} \rangle$, respectively.

The two weighting functions $D_\eta(\omega)$ and $\tilde{D}_\eta(\omega)$ are

given by

$$D_\eta(\omega) = \frac{|\omega|}{\sqrt{\omega^2 - |\Delta_\eta|^2}} \theta(|\omega| - |\Delta_\eta|)$$

$$\tilde{D}_\eta(\omega) = \frac{|\Delta_\eta|}{\sqrt{|\Delta_\eta|^2 - \omega^2}} \theta(|\Delta_\eta| - |\omega|),$$

for the superconducting leads, and $D_\eta(\omega) \equiv 1$ and $\tilde{D}_\eta(\omega) \equiv 0$ if η describes a normal lead.

The current $J_{1\eta}$ involves only excitations energies ω above the gap. This is the only contribution in a normal lead, where it reduces to the result presented in Ref. 33. For a superconducting lead, $J_{1\eta}$ has a contribution due to the normal elements of the dot Green's function, which describes quasiparticle transport and is independent of the superconducting phase difference, and a contribution due to the anomalous components of the Green's functions, which is in general phase dependent.

On the other hand, $J_{2\eta}$ involves only excitations energies ω below the gap and it describes both Josephson as well as Andreev tunneling.

The above current formula becomes particularly useful in the limit of a large superconducting gap ($|\Delta_\eta| \rightarrow \infty$), where quasi-particle excitations are inaccessible, $J_{2\eta}$ dominates the transport. In this case, the current in the superconducting lead η reads

$$J_\eta = -\frac{2e}{\hbar} \Gamma_\eta |\langle d_\downarrow d_\uparrow \rangle| \sin(\Psi - \Phi_\eta), \quad (18)$$

where $\langle d_\downarrow d_\uparrow \rangle = |\langle d_\downarrow d_\uparrow \rangle| \exp(i\Psi)$ is the dot pair amplitude. Equation (18) has a very simple meaning: it describes the Josephson current between the lead with superconducting phase Φ_η and the dot with a phase Ψ . All the complicated physical effects due to the interplay of Coulomb interaction, coupling to all (normal and superconducting) leads and non-equilibrium due to a finite bias voltage between normal and superconducting leads, are hidden in the dot pair amplitude.

III. RESULTS

In the remaining part of the paper, we illustrate our formalism by considering two examples.

A. Josephson coupling due to cotunneling

First, we analyze the equilibrium Josephson current through a superconductor-dot-superconductor system in the limit of weak tunnel coupling. The lowest-order mechanism that establishes a Josephson coupling between the superconductors is cotunneling, i.e. the Josephson current starts in second order in the tunnel-coupling strengths Γ_η . We consider a symmetric setup with both tunnel-coupling strengths equal to Γ_S and $\Delta_L = \Delta_R^* = |\Delta| \exp(i\Phi/2)$. The two superconductors

are kept at the same chemical potential $\mu_S = 0$. We determine the Josephson current $J_{\text{jos}} = J_L = -J_R$ to second order in Γ_S ,

$$J_{\text{jos}} = -\frac{e}{\hbar} \sum_{\chi\chi'\chi''} \left[W_{\chi\chi'}^{\chi\chi''L(2)} P_{\chi'}^{\chi''(0)} + W_{\chi\chi'}^{\chi\chi''L(1)} P_{\chi'}^{\chi''(1)} \right]. \quad (19)$$

For the limit $|\Delta| \gg k_B T$ considered here, there is no microscopic mechanism in our model to make the dot degrees of freedom relax to equilibrium. This situation occurs because the quasiparticles excitation in the superconducting leads are not accessible. In reality, the degrees of freedom of the dot will be coupled to some thermal bath with temperature T and the dot will reach an equilibrium distribution. Hence, we assume that in

zeroth order only the diagonal probabilities are non vanishing and they are given by the Boltzmann factors

$$P_{\chi}^{(0)} = \frac{\exp[-E_{\chi}/(k_B T)]}{Z}, \quad (20)$$

with $E_0 = 0$, $E_{\uparrow} = E_{\downarrow} = \epsilon$, $E_D = 2\epsilon + U$ and $Z = \sum_{\chi} \exp[-E_{\chi}/(k_B T)]$. Notice that in the model studied later in Section III B, the presence of a normal lead tunnel coupled to the dot provides a mechanism for the dot to reach equilibrium. First, we focus on the regime that both ϵ and $\epsilon + U$ lie inside the superconducting gap. The only non-vanishing first-order correction to the reduced density matrix concerns the off-diagonal element $P_D^0 = (P_0^D)^*$ and it reads

$$\begin{aligned} P_D^{0(1)} &= \frac{i}{2\epsilon + U} \left[W_{D0}^{00(1)} P_0^{(0)} + W_{DD}^{0D(1)} P_D^{(0)} + 2W_{D\sigma}^{0\sigma(1)} P_{\sigma}^{(0)} \right] \\ &= \frac{2}{2\epsilon + U} \Gamma_S \cos \frac{\Phi}{2} \left\{ A \left(\frac{\epsilon}{|\Delta|} \right) P_0^{(0)} - A \left(-\frac{\epsilon + U}{|\Delta|} \right) P_D^{(0)} - \left[A \left(-\frac{\epsilon}{|\Delta|} \right) - A \left(\frac{\epsilon + U}{|\Delta|} \right) \right] P_{\sigma}^{(0)} \right\}, \quad (21) \end{aligned}$$

where the function $A(z)$ is given by

$$A(z) = \frac{1}{\pi} \int_1^{\infty} dx \frac{1}{x+z} \frac{1}{\sqrt{x^2-1}}. \quad (22)$$

Equation (21) describes how a finite pair amplitude in the dot can be established in first-order in Γ_S . In fact,

$(P_D^0)^* = P_0^D = \langle d_{\downarrow} d_{\uparrow} \rangle$ is equal to the pair amplitude in the dot.

Evaluating the second-order current diagrams $W_{\chi\chi'}^{\chi\chi''L(2)}$ (an example is shown in Appendix A) and using Eq. (19), we obtain the following lengthy but complete result for the Josephson current

$$\begin{aligned} J_{\text{jos}} &= \frac{2e}{\hbar} \Gamma_S^2 \sin \Phi \left\{ \left[\frac{1}{|\Delta|} F \left(\frac{\epsilon}{|\Delta|} \right) + \frac{2}{2\epsilon + U} A^2 \left(\frac{\epsilon}{|\Delta|} \right) \right] P_0^{(0)} \right. \\ &\quad + \left[\frac{1}{|\Delta|} F \left(-\frac{\epsilon + U}{|\Delta|} \right) - \frac{2}{2\epsilon + U} A^2 \left(-\frac{\epsilon + U}{|\Delta|} \right) \right] P_D^{(0)} \\ &\quad \left. - \frac{1}{|\Delta|} \left[F \left(-\frac{\epsilon}{|\Delta|} \right) + F \left(\frac{\epsilon + U}{|\Delta|} \right) + 4B \left(\frac{-\epsilon}{|\Delta|}, \frac{\epsilon + U}{|\Delta|} \right) \right] P_{\sigma}^{(0)} \right\}, \quad (23) \end{aligned}$$

where the functions $F(z)$ and $B(z, z')$ are defined as

$$F(z) = \frac{1}{\pi^2} \int_1^{\infty} dx \frac{1}{\sqrt{x^2-1}} \int_1^{\infty} dy \frac{1}{\sqrt{y^2-1}} \frac{1}{x+z} \frac{1}{x+y} \frac{1}{y+z} \quad (24a)$$

$$B(z, z') = \frac{1}{\pi^2} \int_1^{\infty} dx \frac{1}{\sqrt{x^2-1}} \int_1^{\infty} dy \frac{1}{\sqrt{y^2-1}} \frac{1}{x+z} \frac{1}{x+y} \frac{1}{x+z'}. \quad (24b)$$

In the limit $|\Delta| \rightarrow \infty$, all second-order current rates vanish and the Josephson current is given by $P_0^{D(1)}$ multiplied by the corresponding first-order current rates, which yields

$$J_{\text{jos}} = \frac{e}{\hbar} \Gamma_S^2 \sin \Phi \frac{1}{2\epsilon + U} \left(P_0^{(0)} - P_D^{(0)} \right). \quad (25)$$

The result Eq. (23) for the second-order equilibrium Josephson current is valid when both the level ϵ and $\epsilon + U$ are inside the gap, therefore the limit of large interaction $U \rightarrow \infty$ cannot be obtained directly from Eq. (23). However, in the limit of large interaction the double occupa-

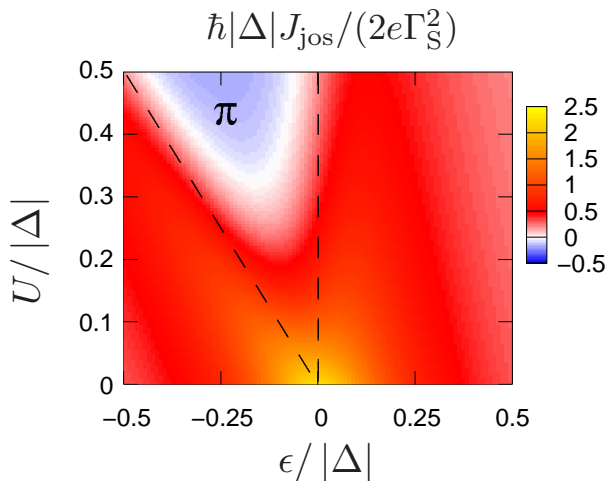


FIG. 2: (Color online) Density plot of the Josephson current as a function of the level position ϵ and of the interaction strength U . The region where the system behaves as a π -junction is indicated by the symbol π in the plot. The dashed lines delimit the region where at zero temperature the dot is singly occupied. The other parameters used in the simulation are: $k_B T/|\Delta| = 0.05$, $\Gamma_S/|\Delta| = 0.01$, $\Phi = \pi/2$.

tion of the dot is forbidden, and the Josephson current can be obtained by dropping all diagrams involving the doubly occupied state $|D\rangle$:

$$\begin{aligned} J_{\text{jos}} &= -\frac{e}{\hbar} \left[W_{00}^{00L(2)} P_0^{(0)} + 2W_{\sigma\sigma}^{\sigma\sigma L(2)} P_\sigma^{(0)} \right] \\ &= \frac{2e}{\hbar} \frac{\Gamma_S^2}{|\Delta|} \sin \Phi \left[F\left(\frac{\epsilon}{|\Delta|}\right) P_0^{(0)} - F\left(-\frac{\epsilon}{|\Delta|}\right) P_\sigma^{(0)} \right] \end{aligned}$$

Equation (26) agrees with the results of Glazman and Matveev.¹¹

The Josephson current, Eq. (23), is plotted in Fig. 2 as a function of gate voltage and interaction strength. We find, in agreement with Ref. 2, the formation of a π -state for gate voltages such that $-U \lesssim \epsilon \lesssim 0$, with the transitions being smeared out by temperature.

B. Andreev-level spectroscopy

We now turn our attention to the setup shown in Fig. 3. As compared to the geometry considered so far, there is a third, normal (N), lead with tunnel-coupling strength Γ_N , in addition to the two superconducting ones (L, R). Again, we assume the same tunnel coupling Γ_S and chemical potential $\mu_S = 0$ for both superconducting leads, and $\Delta_L = \Delta_R^* = |\Delta| \exp(i\Phi/2)$. The third lead allows for driving the quantum dot out of equilibrium by applying a voltage between normal and superconducting leads, expressed by a non vanishing chemical potential μ_N of the normal lead. The quantities of interest are the Josephson current $J_{\text{jos}} = (J_L - J_R)/2$ and the Andreev current in the normal lead $J_{\text{and}} = -(J_R + J_L)$.

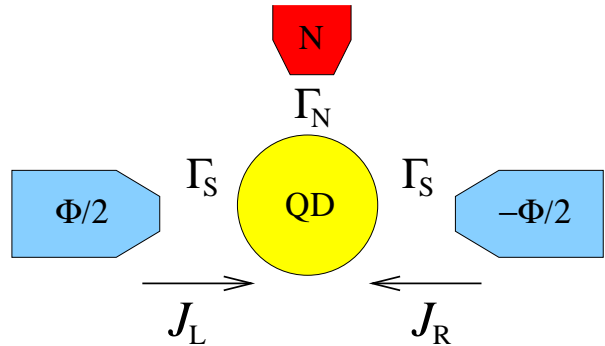


FIG. 3: Schematic setup of a quantum dot tunnel coupled to one normal and two superconducting leads. The dot can be driven out of equilibrium by a bias voltage applied to the normal lead.

In Ref. 29 we studied this setup in the limit of weak tunnel couplings. We found that by applying a bias voltage between normal and superconducting leads one can induce an out-of-equilibrium proximity effect in the quantum dot, which, in turn, supports a Josephson coupling carried by first-order tunnel processes instead of second order (cotunneling). We described the non-equilibrium Josephson current as well as transitions from 0 to π -states perturbatively to first order in Γ_S . This limited the applicability to a small range of gate voltages and temperatures larger than the tunnel-coupling strengths. The proximity effect was of purely non-equilibrium origin since the influence of the superconducting leads on the quantum-dot spectrum, typically associated with the picture of Andreev bound states, could not be resolved.

In the present paper, we want to go beyond the limit considered in Ref. 29 for two reasons. First, we aim at covering the full range of gate and bias voltages, thus, including both equilibrium and non-equilibrium proximity effect. Second, we are interested in mapping out the spectrum of Andreev bound states of an interacting quantum dot. To pursue both of these aims, we need to go beyond first-order transport in Γ_S . As usual for interacting systems, the full problem for arbitrary values of $|\Delta|$ and Γ_S can only be solved approximatively. In the limit of a large superconducting gap $|\Delta| \rightarrow \infty$, however, we are able to derive an exact result by resummation of the contributions of all orders in Γ_S . This is possible because for $|\Delta| \rightarrow \infty$ only a small subset of all diagrams contributes to the generalized rates: the only superconducting lines that remain are anomalous ones that connect vertices within one (the upper or the lower) propagator, with no other vertex appearing in between. This simplification is related to the inaccessibility of quasiparticle excitations in the superconducting leads and the fact that a Cooper pair should tunnel in a time interval $\propto \hbar/|\Delta|$, which becomes infinitesimal for $|\Delta| \rightarrow \infty$. A rigorous proof is given in Appendix B.

In the limit $|\Delta| \rightarrow \infty$ we can evaluate the current in the superconducting leads L, R by means of Eq. (18), i.e., we only need the pair amplitude of the quantum dot. It is useful to introduce a dot isospin defined as²⁹

$$I_x = \frac{P_0^D + P_D^0}{2}; I_y = i \frac{P_0^D - P_D^0}{2}; I_z = \frac{P_D - P_0}{2}. \quad (27)$$

Finite x - and y -components of the isospin indicate coherent superpositions of the dot being empty or doubly-occupied.

We rewrite the master equation for the dot reduced density matrix in the form of a Bloch equation for the isospin, taking into account all rates up to first order in Γ_N [the order in Γ_N is indicated by the superscript (i) with $i = 0, 1$]. The Bloch equation for the isospin reads:

$$0 = \frac{d\mathbf{I}}{dt} = \mathbf{A} - \mathbf{R} \cdot \mathbf{I} + \mathbf{I} \times \mathbf{B}, \quad (28)$$

where the first, second, and third term describe generation, relaxation, and rotation of the isospin, respectively. The explicit expressions of the needed generalized rates are reported in Appendix D. In order to decouple the equations for the isospin from those for the diagonal probabilities we made use of the relations: $W_{D\sigma}^{(1)} + W_{\sigma D}^{(1)} - W_{0\sigma}^{(1)} - W_{\sigma 0}^{(1)} = 0$ and $2W_{0\sigma}^{D\sigma(1)} - W_{00}^{D0(1)} - W_{0D}^{DD(1)} = 0$. The relaxation tensor and the generation vector start in first order in Γ_N . The generation vector reads

$$\mathbf{A}^{(1)} = \begin{pmatrix} \text{Re} \left\{ W_{0\sigma}^{D\sigma(1)} \right\} \\ -\text{Im} \left\{ W_{0\sigma}^{D\sigma(1)} \right\} \\ \frac{1}{2} \left(W_{D\sigma}^{(1)} - W_{0\sigma}^{(1)} \right) \end{pmatrix}. \quad (29)$$

The only non vanishing elements of the relaxation tensor are: $R_{xx}^{(1)} = R_{yy}^{(1)} = -\text{Re} \left\{ W_{00}^{DD(1)} \right\}$, $R_{zz}^{(1)} = W_{\sigma 0}^{(1)} + W_{\sigma D}^{(1)}$, and $R_{xz}^{(1)} = R_{zx}^{(1)} = \text{Re} \left\{ W_{00}^{0D(1)} - W_{D0}^{DD(1)} \right\}$. The effec-

tive magnetic field acting on the isospin has a zeroth-order component $\mathbf{B}^{(0)}$ and a first-order component $\mathbf{B}^{(1)}$,

$$\mathbf{B}^{(0)} = \begin{pmatrix} 2\Gamma_S \cos \Phi/2 \\ 0 \\ -(2\epsilon + U) \end{pmatrix} \quad (30)$$

$$\mathbf{B}^{(1)} = \begin{pmatrix} -\text{Im} \left\{ W_{D0}^{DD(1)} - W_{00}^{0D(1)} \right\} \\ 0 \\ \text{Im} \left\{ W_{00}^{DD(1)} \right\} \end{pmatrix}. \quad (31)$$

The explicit expressions for the generation vector and the relaxation tensor can be written in a compact way, if we define the Andreev bound-state energies. These are given by the poles of the retarded Green's function of the dot for vanishing coupling to the normal lead,

$$E_{A,\gamma',\gamma} = \gamma' \frac{U}{2} + \gamma \sqrt{\left(\epsilon + \frac{U}{2} \right)^2 + \Gamma_S^2 \cos^2 \frac{\Phi}{2}}, \quad (32)$$

where γ and γ' can take the values ± 1 . There are four resonances which lie pairwise around zero energy. We get for the generation vector:

$$A_x^{(1)} = -\frac{\Gamma_S \Gamma_N}{4\epsilon_A} \cos \frac{\Phi}{2} \sum_{\gamma,\gamma'=\pm} \gamma f_N(E_{A,\gamma',\gamma}) \quad (33a)$$

$$A_y^{(1)} = 0 \quad (33b)$$

$$A_z^{(1)} = \frac{\Gamma_N}{4} \sum_{\gamma,\gamma'=\pm} \left(1 + \gamma \frac{\epsilon + U/2}{\epsilon_A} \right) \left[f_N(E_{A,\gamma',\gamma}) - \frac{1}{2} \right] \quad (33c)$$

with $\epsilon_A = \sqrt{\left(\epsilon + \frac{U}{2} \right)^2 + \Gamma_S^2 \cos^2 \frac{\Phi}{2}}$, where the square-root dependence clearly indicates that the result is non-perturbative in Γ_S . The non-vanishing elements of the relaxation tensor are:

$$R_{xx}^{(1)} = R_{yy}^{(1)} = \frac{\Gamma_N}{2} \sum_{\gamma,\gamma'=\pm} \left(1 - \gamma \frac{\epsilon + U/2}{\epsilon_A} \right) \left[\frac{1}{2} - \gamma' f_N(E_{A,\gamma',\gamma}) \right] \quad (34a)$$

$$R_{zz}^{(1)} = \frac{\Gamma_N}{2} \sum_{\gamma,\gamma'=\pm} \left(1 + \gamma \frac{\epsilon + U/2}{\epsilon_A} \right) \left[\frac{1}{2} - \gamma' f_N(E_{A,\gamma',\gamma}) \right] \quad (34b)$$

$$R_{xz}^{(1)} = R_{zx}^{(1)} = \frac{\Gamma_S \Gamma_N}{2\epsilon_A} \cos \frac{\Phi}{2} \sum_{\gamma,\gamma'=\pm} \gamma \gamma' f_N(E_{A,\gamma',\gamma}). \quad (34c)$$

By means of Eq. (18), the current in the superconducting leads can be written as $J_{R,L} = \frac{2e}{\hbar} \Gamma_S \left(I_y \cos \frac{\Phi}{2} \mp I_x \sin \frac{\Phi}{2} \right)$, where the upper (lower) sign refers to the right (left) lead. Hence, the x - and y -

component of the isospin provide the Josephson and An-

dreev currents, respectively,

$$J_{\text{j os}} = \frac{2e}{\hbar} \Gamma_S I_x \sin \frac{\Phi}{2} \quad (35)$$

$$J_{\text{and}} = -\frac{4e}{\hbar} \Gamma_S I_y \cos \frac{\Phi}{2}, \quad (36)$$

whereas the z -component is related to the charge in the quantum dot,

$$Q = -e(1 + 2I_z). \quad (37)$$

We solve for the stationary solution for the isospin. Expanding the Eq. (28) to zeroth order in Γ_N yields $0 = \mathbf{I}^{(0)} \times \mathbf{B}^{(0)}$, and, thus, $\mathbf{I}^{(0)} \parallel \mathbf{B}^{(0)}$. To determine the proportionality constant, we multiply $\mathbf{B}^{(0)}$ from the left to Eq. (28) expanded to first order in Γ_N , and obtain the zeroth-order result

$$\mathbf{I}^{(0)} = \left(\frac{\mathbf{A}^{(1)} \cdot \mathbf{B}^{(0)}}{\mathbf{B}^{(0)} \cdot \mathbf{R}^{(1)} \cdot \mathbf{B}^{(0)}} \right) \mathbf{B}^{(0)}, \quad (38)$$

which yields the Josephson current and the quantum-dot charge. The Andreev current, on the other hand, is proportional to the y -component of the isospin and starts in first order in Γ_N . The first-order contribution to the y -component of the isospin can be derived by multiplying either $\hat{\mathbf{x}}$ or $\hat{\mathbf{z}}$ from the left to Eq. (28) expanded to first order

$$I_y^{(1)} = \frac{1}{B_x^{(0)}} \hat{\mathbf{z}} \cdot (\mathbf{A}^{(1)} - \mathbf{R}^{(1)} \cdot \mathbf{I}^{(0)}) \quad (39)$$

$$= -\frac{1}{B_z^{(0)}} \hat{\mathbf{x}} \cdot (\mathbf{A}^{(1)} - \mathbf{R}^{(1)} \cdot \mathbf{I}^{(0)}). \quad (40)$$

The formation of a finite pair amplitude of the dot is favored if the empty and doubly-occupied dot states are degenerate, $2\epsilon + U = 0$. In this case, however, the dot is preferably singly occupied in equilibrium, i.e., the proximity effect is strongly suppressed by Coulomb charging. For finite values of the superconducting gap $|\Delta|$, a small Josephson current through the dot can be established by cotunneling processes. In the limit of infinite $|\Delta|$, however, this is not possible, and the proximity effect and, thus, the Josephson current is exponentially suppressed. In fact, we find for this regime $\mathbf{A}^{(1)} = 0$, i.e., no isospin is generated.

There are two routes towards the generation of a finite dot pair amplitude. One is to change the gate voltage such that empty or double occupation of the dot becomes available. Then, the tunnel coupling to the superconductors give rise to an equilibrium proximity effect that, however, starts in higher order in the tunnel coupling strength. To achieve a finite pair amplitude at lowest order already, one has to apply a finite bias voltage at the normal lead. This induces a non-equilibrium proximity effect that supports a first-order Josephson current through the dot.

1. Equilibrium

First, we consider the equilibrium situation ($\mu_N = 0$). In this case, the relation $\hat{\mathbf{x}} \cdot \mathbf{R}^{(1)} \cdot \mathbf{B}^{(0)} / \hat{\mathbf{z}} \cdot \mathbf{R}^{(1)} \cdot \mathbf{B}^{(0)} = A_x^{(1)} / A_z^{(1)}$ ensures that no current flows in the normal lead. The exact result for the equilibrium Josephson current in zeroth order in Γ_N reads

$$J_{\text{j os}} = \frac{e}{\hbar} \Gamma_S^2 \sin \Phi \frac{\sum_{\gamma, \gamma' = \pm} (1 + \gamma \frac{\epsilon + U/2}{\epsilon_A}) [f(E_{A, \gamma', \gamma}) - \frac{1}{2}]}{(2\epsilon + U) \sum_{\gamma, \gamma' = \pm} (1 + \gamma \frac{\epsilon + U/2}{\epsilon_A}) [\gamma' f(E_{A, \gamma', \gamma}) - \frac{1}{2}] + \frac{2}{\epsilon_A} \Gamma_S^2 \cos^2(\Phi/2) \sum_{\gamma, \gamma' = \pm} \gamma \gamma' f(E_{A, \gamma', \gamma})}, \quad (41)$$

where $f(\omega)$ is the Fermi function with zero chemical potential. Notice that the only role played by the normal lead is to provide a mechanism for the electrons in the dot to reach equilibrium. Expanding Eq. (41) to second order in Γ_S we recover the result of Eq. (25).

In equilibrium, the pair amplitude of the quantum dot $\langle d_{\downarrow} d_{\uparrow} \rangle$ for the symmetric setup and symmetric gauge is real, i.e. $\langle d_{\downarrow} d_{\uparrow} \rangle = I_x$ since $I_y = 0$. In panel (a) of Fig. 4 we plot the pair amplitude as a function of the level position ϵ for zero temperature. In particular we note that a quantum phase transition occurs if $U/2 > \Gamma_S |\cos(\Phi/2)|$ at $\epsilon = \bar{\epsilon}_{\pm} = -U/2 \pm \sqrt{(U/2)^2 - \Gamma_S^2 \cos^2(\Phi/2)}$. The values $\bar{\epsilon}_{\pm}$ where the transition takes place depend on the tunnel coupling Γ_S and on the superconducting phase difference. The pair amplitude in first order Γ_S , see Eq. (21), which

gives rise to the second-order Josephson current, exhibits the phase transition at different values of the level position. The behavior of the pair amplitude can be understood by considering the Andreev-bound-state configuration in each region (see inset of panel (a) of Fig. 4). Panel (b) of Fig. 4 shows the charge of the dot as a function of the level position. In this case, the first-order Γ_S correction vanishes. The full result for the charge shows that due to proximity effect the charge on the dot is not always quantized.²³

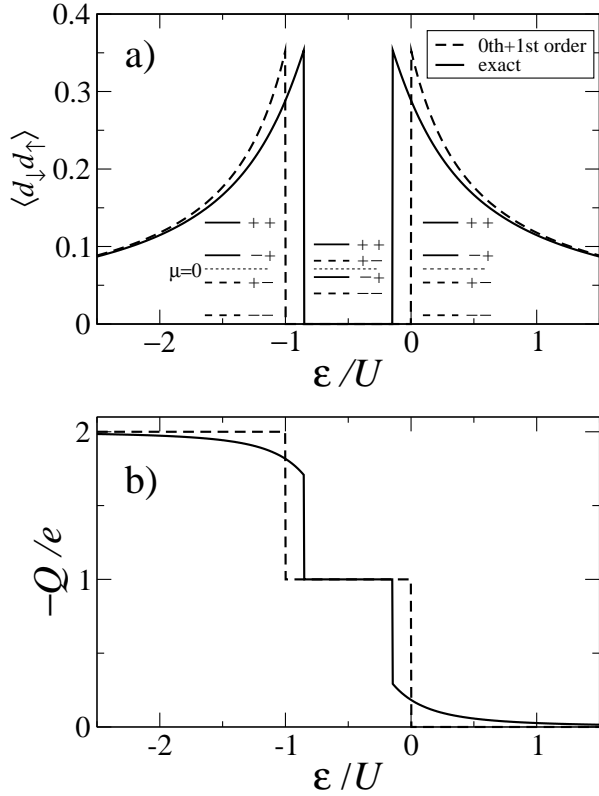


FIG. 4: Dot pair amplitude $\langle d_{\downarrow}d_{\uparrow} \rangle$ (a) and charge (b) as a function of the level position ϵ at zero temperature. Note that the pair amplitude in equilibrium for the symmetric setup is real. The dashed lines refer to the pair amplitude and charge calculated up to first-order in Γ_S ; for the pair amplitude the 0th-order contribution vanishes, while for the charge the first-order one does. In the inset of panel a) we show a schematic picture of the Andreev bound state energies $E_{A,\gamma',\gamma}$ in the three different regions, where the values $\gamma' \gamma$ are indicated next to the level. The sign of the contributions of the bound states $E_{A,\gamma',\gamma}$ to $\langle d_{\downarrow}d_{\uparrow} \rangle$ is determined by the index γ . We have depicted the levels with $\gamma = +$ by a solid line and those with $\gamma = -$ by a dashed line. The other parameters used in the simulation are: $\Gamma_S/U = 0.5$, and $\Phi = \pi/2$.

2. Non-equilibrium

Next we turn our attention to the non-equilibrium situation ($\mu_N \neq 0$). Applying a bias voltage to the normal lead produces a finite current in N, which is sustained by Andreev-reflection processes. We do not give here the explicit analytical expressions for the zeroth-order J_{jos} and the first-order J_{and} since they are rather lengthy. Instead, in Figs. 5, 6, 7 we plot the Josephson current, the Andreev current, and the dot charge as a function of the level position ϵ and of the chemical potential of the normal lead μ_N , for different values of the tunnel-coupling with the superconductor.

In Fig. 5(a) one can see how the Josephson current can be controlled by the chemical potential of the nor-

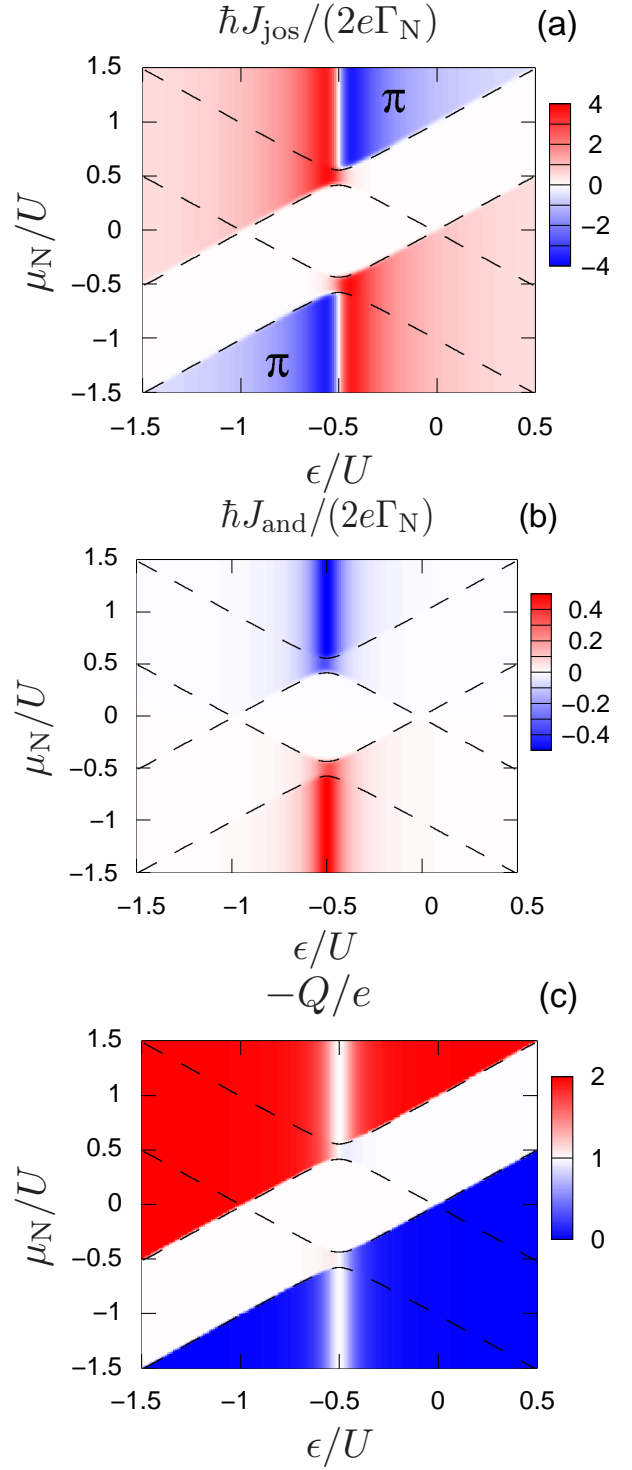


FIG. 5: (Color online) Density plot of the Josephson current (a), the Andreev current (b), and the charge on the quantum dot (c) as a function of the level position ϵ and of the chemical potential μ_N . In panel (a), the region where the system behaves as a π -junction is indicated by the symbol π . The dashed lines map the Andreev bound states: $\mu_N = E_{A,\gamma',\gamma}$. The other parameters used in the simulation are: $k_B T/U = 0.01$, $\Gamma_N/U = 0.005$, $\Gamma_S/U = 0.1$, and $\Phi = \pi/2$.

mal lead. There is, first, a broad region set by the charging energy in which the Josephson current is suppressed. Second, a π -transition can be driven both by the transport voltage and by the gate voltage controlling the level position. For fixed μ_N the transition occurs at $\epsilon = -U/2$, i.e. when the energy of the empty and double occupied dot are degenerate. We remark that this transition is slightly shifted when higher-order corrections to the effective field are included. In fact, near the transition $B_z^{(0)} = 2\epsilon + U$ becomes small and hence $B_z^{(1)}$ needs to be taken into account. This has been done in Ref. 29 in the weak-proximity limit. Panel (b) of Fig. 5 shows the Andreev current. It is largest at $\epsilon = -U/2$ outside the region where charging energy suppresses transport. Panel (c) of Fig. 5 shows the dot charge. We find a pronounced feature around $\epsilon = -U/2$ that is associated with generating a y -component of the isospin by rotation out of the z -direction.

In Figs. 6 and 7, the coupling to the superconducting lead is stronger, comparable to the Coulomb interaction strength, and the term proportional to Γ_S in $\sqrt{(\epsilon + U/2)^2 + \Gamma_S^2 \cos^2(\Phi/2)}$ becomes more important, leading to a more pronounced splitting of the Andreev bound-state energies. We stress here that the current in the normal lead as a function of both gate and transport voltage maps the energies of the Andreev bound states in the dot. Therefore, measuring the current in the normal lead allows to perform a *an Andreev-bound-state spectroscopy* and, hence, to gather information on the superconducting correlations induced in the dot.

IV. CONCLUSION

We have presented a real-time diagrammatic transport theory for systems composed of interacting quantum dots coupled both to normal and superconducting leads. First, we have applied this theory to study the Josephson current through a quantum-dot tunnel coupled to two superconductors in second order in the tunnel-coupling strengths. In particular, we have studied how a π -phase develops with increasing on-site Coulomb repulsion. Next, we have considered a quantum dot coupled to one normal and two superconducting leads, in the limit of large superconducting gap. In this regime, all orders in the tunnel-coupling strengths with the superconductors can be summed. This enabled us to investigate the strong-proximity regime. In particular, we analyze the Josephson current and identify the parameter regions where the system behaves as π -junction; the π -transition can be triggered both by the dot level position and the bias voltage. We find also that a spectroscopy of the Andreev bound states of the system can be realized by measuring the Josephson current between the two superconductors, the Andreev current in the normal lead or the charge of the dot as a function of both the dot level-position and the bias voltage.

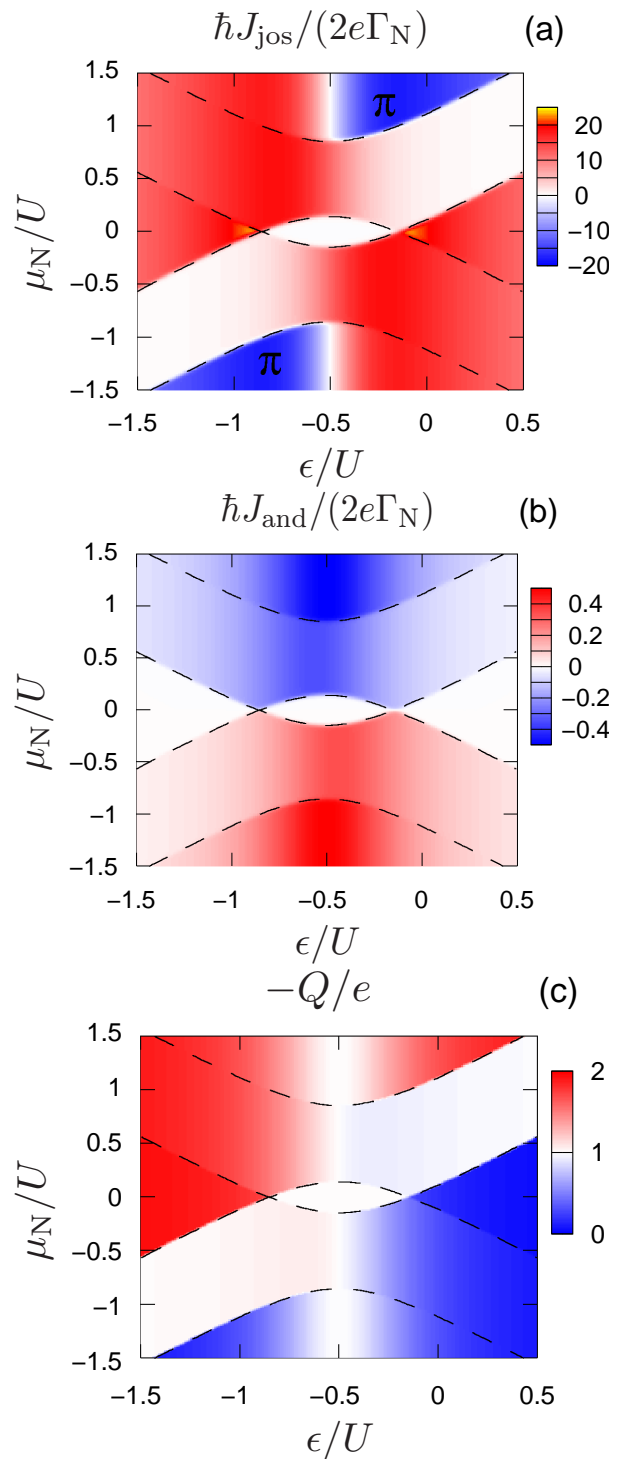


FIG. 6: (Color online) Density plot of the Josephson current (a), the Andreev current (b), and the charge on the quantum dot (c) as a function of the level position ϵ and of the chemical potential μ_N . In panel (a), the region where the system behaves as a π -junction is indicated by the symbol π . The dashed lines map the Andreev bound states: $\mu_N = E_{A,\gamma',\gamma}$. The other parameters used in the simulation are: $k_B T/U = 0.01$, $\Gamma_N/U = 0.005$, $\Gamma_S/U = 0.5$, and $\Phi = \pi/2$.

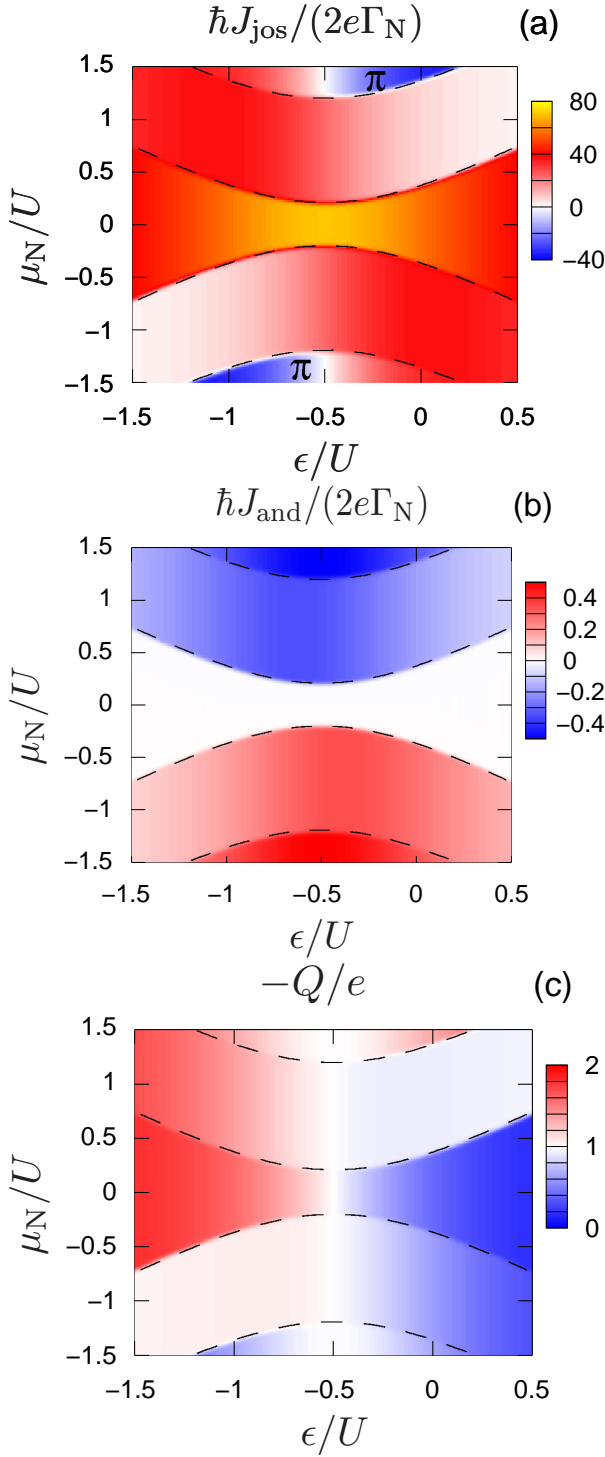


FIG. 7: (Color online) Density plot of the Josephson current (a), the Andreev current (b), and the charge on the quantum dot (c) as a function of the level position ϵ and of the chemical potential μ_N . In panel (a), the region where the system behaves as a π -junction is indicated by the symbol π . The dashed lines map the Andreev bound states: $\mu_N = E_{A,\gamma',\gamma}$. The other parameters used in the simulation are: $k_B T/U = 0.01$, $\Gamma_N/U = 0.005$, $\Gamma_S/U = 1$, and $\Phi = \pi/2$.

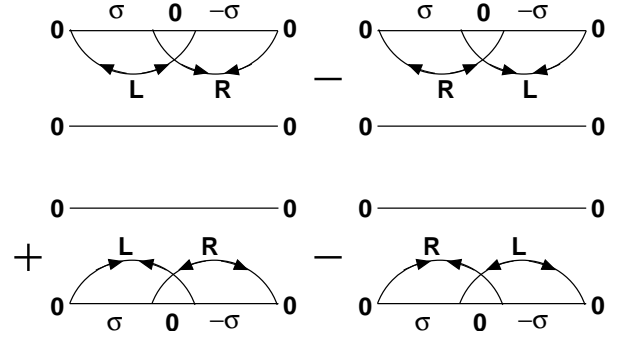


FIG. 8: Second-order diagrams contributing to the current rate $W_{00}^{00L(2)}$.

Acknowledgments

We would like to thank W. Belzig, F. S. Bergeret, R. Fazio, A. Shmirman, and A. Volkov for useful discussions. Financial support from the DFG via SFB 491 is acknowledged.

APPENDIX A: SECOND-ORDER, FINITE $|\Delta|$

In this Appendix we show, as an example, the calculation of the second-order current rate $W_{00}^{00L(2)}$. The second-order diagrams contributing to this rate are shown in Fig. 8; the signs have been assigned making use of Rule 6 in Section II B 3. Using the diagrammatic rules of Section II B 3 we get

$$\begin{aligned}
W_{00}^{00L(2)} &= -8\Gamma_S^2 \sin \Phi \int_{|\Delta|}^{\infty} \frac{d\omega}{2\pi} \frac{|\Delta|}{\sqrt{\omega^2 - |\Delta|^2}} \int_{|\Delta|}^{\infty} \frac{d\omega'}{2\pi} \frac{|\Delta|}{\sqrt{\omega'^2 - |\Delta|^2}} \frac{1}{\omega + \epsilon} \frac{1}{\omega + \omega'} \frac{1}{\omega' + \epsilon} \\
&= -2 \frac{\Gamma_S^2}{|\Delta|} \sin \Phi F \left(\frac{\epsilon}{|\Delta|} \right)
\end{aligned}$$

APPENDIX B: DERIVATION OF THE RULES FOR $|\Delta| \rightarrow \infty$

Here, we give a rigorous proof of the rules which in the $|\Delta| \rightarrow \infty$ limit allow us to greatly reduce the number of diagrams to be considered.

Rule (i): *No vertex should be considered between the two vertices of a line with a superconducting lead.*

Let us consider a diagram where a vertex v' exists between the two vertices of a superconducting line with energy ω . Let the vertex v' be associated with a line with energy ω' . According to the diagrammatic rules 2 and 3, this diagram contains the factor³⁵ $\frac{1}{\pm\omega\dots} \frac{1}{\pm\omega\pm\omega'\dots} D(\omega) |\Delta/\omega|$ which upon integration over ω vanishes as $1/|\Delta|$. On the other hand, if no vertex is inserted between the two vertices of the superconducting line, the diagram contains the factor³⁵ $\frac{1}{\pm\omega\dots} D(\omega) |\Delta/\omega|$ which remains finite upon integration over ω .

Rule (ii): *No line with a superconductor joining the upper and lower propagator should be considered.*

Let us consider the diagram where a superconducting line is running from the upper to the lower propagator and the vertex on the upper propagator is on the left of the one on the lower propagator. In virtue of rule (i), the diagram with the two vertices swapped, i.e. with the vertex on the upper propagator being on the right of the one on the lower propagator, also exists. These two diagrams cancel each other for $|\Delta| \rightarrow \infty$.

Rule (iii): *No normal line with a superconductor should be considered.*

Let us consider a part of a diagram with a state $|\chi_u\rangle$ running on the upper part of the Keldysh contour and with a state $|\chi_l\rangle$ on the lower part. In virtue of the two previous rules, there are only four possible ways of inserting a normal line with a superconducting lead, which are schematically depicted in Fig. 9. In the large-gap limit, the diagrams corresponding to the possible insertion of a normal line, have the same absolute value. But the diagrams arising from the insertion in the lower propagator (shown in the second line of Fig. 9) have an opposite sign with respect to the ones in the upper propagator (first line of Fig. 9). Finally, it is easy to prove that for any $|\chi_u\rangle$ and $|\chi_l\rangle$ there are, for our single-level model, only four

possible insertions: two in the upper propagator and two in the lower propagator. Hence, the sum of all these diagrams vanishes. To clarify this point, let us consider the exemplary case that $|\chi_u\rangle = |0\rangle$ and $|\chi_l\rangle = |\uparrow\rangle$: then the possible insertions are: (a) with intermediate state $|\uparrow\rangle$

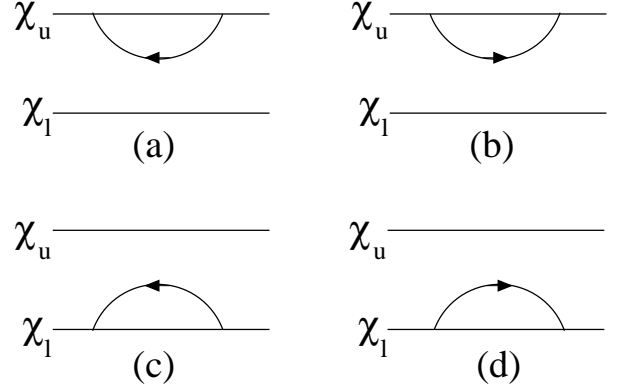


FIG. 9: Possible insertion of a normal line in the upper or in the lower propagator. Note that these insertions are a part of a larger irreducible diagram and hence there are other lines (not shown) running from one side to the other of the insertion.

or $|\downarrow\rangle$ for the upper propagator; (c) with intermediate state $|0\rangle$ and (d) with intermediate state $|D\rangle$ for the lower propagator.

APPENDIX C: CALCULATION OF A GENERALIZED RATE IN THE $|\Delta| \rightarrow \infty$ LIMIT

Here, we show in one example how all contributions in Γ_S can be summed up. We consider the off-diagonal rate $W_{00}^{D0(1)}$ in first order in Γ_N and we add all contributions in Γ_S . In particular, only diagrams with an odd number of anomalous lines on the upper propagator contribute to this rate. The first two diagrams are shown in Fig. 10. The contribution with $2n + 1$ anomalous line reads

$$2i\Gamma_N \int \frac{d\omega}{2\pi} f_N(\omega) \left(\frac{1}{-\omega + \epsilon + i0^+} \cdot \frac{1}{-\omega + \epsilon - U + i0^+} \right)^{n+1} \left(\Gamma_S \cos \frac{\Phi}{2} \right)^{2n+1}.$$

Summing up all terms we get

$$\begin{aligned}
W_{00}^{\text{D0}(1)} &= 2i\Gamma_{\text{N}}\Gamma_{\text{S}} \cos \frac{\Phi}{2} \int \frac{d\omega}{2\pi} f_{\text{N}}(\omega) \frac{1}{(\omega - \epsilon - i0^+)(\omega - \epsilon + U - i0^+) - (\Gamma_{\text{S}} \cos(\Phi/2))^2} \\
&= i \frac{\Gamma_{\text{N}}\Gamma_{\text{S}}}{\epsilon_{\text{A}}} \cos \frac{\Phi}{2} \int \frac{d\omega}{2\pi} f_{\text{N}}(\omega) \left(\frac{1}{\omega + U/2 - \epsilon_{\text{A}} - i0^+} - \frac{1}{\omega + U/2 + \epsilon_{\text{A}} - i0^+} \right),
\end{aligned}$$

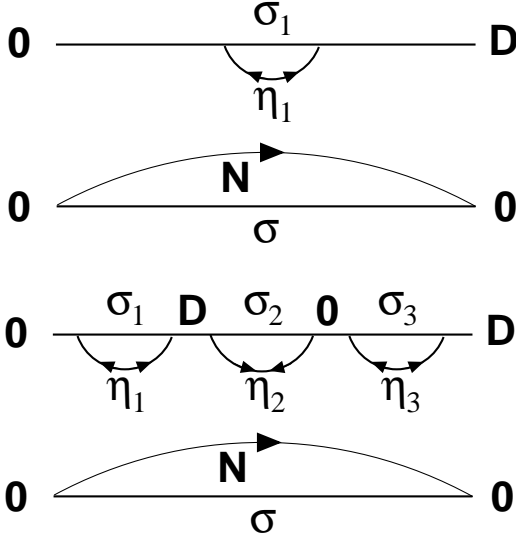


FIG. 10: First two contributions to $W_{00}^{\text{D0}(1)}$.

with $\epsilon_{\text{A}} = \sqrt{(\epsilon + U/2)^2 + \Gamma_{\text{S}}^2 \cos^2(\Phi/2)}$.

APPENDIX D: GENERALIZED RATES TO ALL ORDERS IN Γ_{S}

In this Appendix we give the expression for the generalized rates, which are necessary to compute the Josephson current in zeroth-order Γ_{N} and the Andreev current in first order. The diagonal rates start in first-order Γ_{N} and they are given by

$$W_{0\sigma}^{(1)} = \frac{\Gamma_{\text{N}}}{2} \sum_{\gamma=\pm} \left(1 + \gamma \frac{\epsilon + U/2}{\epsilon_{\text{A}}} \right) [1 - f_{\text{N}}(E_{\text{A},-\gamma})]$$

$$W_{\sigma 0}^{(1)} = \frac{\Gamma_{\text{N}}}{2} \sum_{\gamma=\pm} \left(1 + \gamma \frac{\epsilon + U/2}{\epsilon_{\text{A}}} \right) f_{\text{N}}(E_{\text{A},-\gamma})$$

$$W_{\sigma \text{D}}^{(1)} = \frac{\Gamma_{\text{N}}}{2} \sum_{\gamma=\pm} \left(1 + \gamma \frac{\epsilon + U/2}{\epsilon_{\text{A}}} \right) [1 - f_{\text{N}}(E_{\text{A},+\gamma})]$$

$$W_{\text{D}\sigma}^{(1)} = \frac{\Gamma_{\text{N}}}{2} \sum_{\gamma=\pm} \left(1 + \gamma \frac{\epsilon + U/2}{\epsilon_{\text{A}}} \right) f_{\text{N}}(E_{\text{A},+\gamma}),$$

where the Andreev bound-state energies read

$$E_{\text{A},\gamma',\gamma} = \gamma' \frac{U}{2} + \gamma \sqrt{\left(\epsilon + \frac{U}{2} \right)^2 + \Gamma_{\text{S}}^2 \cos^2 \frac{\Phi}{2}}.$$

Some of the off-diagonal rates start in zeroth-order Γ_{N} . In particular, we have $W_{00}^{\text{D0}(0)} = (W_{\text{D0}}^{\text{00}(0)})^* = W_{00}^{\text{0D}(0)} = (W_{\text{0D}}^{\text{00}(0)})^* = (W_{\text{0D}}^{\text{DD}(0)})^* = W_{\text{DD}}^{\text{0D}(0)} = (W_{\text{D0}}^{\text{DD}(0)})^* = W_{\text{DD}}^{\text{D0}(0)} = i\Gamma_{\text{S}} \cos \Phi/2$. We also need the real part of the first-order corrections to these rates. Notice that the following relations hold $\text{Re} \{ W_{00}^{\text{D0}(1)} \} = \text{Re} \{ W_{\text{D0}}^{\text{00}(1)} \} = \text{Re} \{ W_{00}^{\text{0D}(1)} \} = \text{Re} \{ W_{\text{0D}}^{\text{00}(1)} \}$ and $\text{Re} \{ W_{\text{0D}}^{\text{DD}(1)} \} = \text{Re} \{ W_{\text{DD}}^{\text{0D}(1)} \} = \text{Re} \{ W_{\text{D0}}^{\text{DD}(1)} \} = \text{Re} \{ W_{\text{DD}}^{\text{D0}(1)} \}$. The first-order corrections read

$$\text{Re} \{ W_{00}^{\text{D0}(1)} \} = -\Gamma_{\text{S}} \cos \frac{\Phi}{2} \frac{\Gamma_{\text{N}}}{2\epsilon_{\text{A}}} \sum_{\gamma=\pm} \gamma f_{\text{N}}(E_{\text{A},-\gamma})$$

$$\text{Re} \{ W_{\text{0D}}^{\text{DD}(1)} \} = -\Gamma_{\text{S}} \cos \frac{\Phi}{2} \frac{\Gamma_{\text{N}}}{2\epsilon_{\text{A}}} \sum_{\gamma=\pm} \gamma f_{\text{N}}(E_{\text{A},+\gamma}).$$

There are also some off-diagonal rates which start in first order in Γ_{N} :

$$\begin{aligned} \operatorname{Re} \left\{ W_{0\sigma}^{\text{D}\sigma(1)} \right\} &= -\operatorname{Re} \left\{ W_{\sigma 0}^{\sigma\text{D}(1)} \right\} = -\frac{\Gamma_S \Gamma_N}{4\epsilon_A} \cos \frac{\Phi}{2} \sum_{\gamma, \gamma' = \pm} \gamma f_N(E_{A, \gamma', \gamma}) \\ \operatorname{Re} \left\{ W_{00}^{\text{DD}(1)} \right\} &= \operatorname{Re} \left\{ W_{\text{DD}}^{00(1)} \right\} = \frac{\Gamma_N}{2} \sum_{\gamma, \gamma' = \pm} \left(1 - \gamma \frac{\epsilon + U/2}{\epsilon_A} \right) \left[\gamma' f_N(E_{A, \gamma', \gamma}) - \frac{1}{2} \right]. \end{aligned}$$

-
- ¹ M. R. Buitelaar, T. Nussbaumer, and C. Schönenberger, Phys. Rev. Lett. **89**, 256801 (2002); J.-P. Cleuziou, W. Wernsdorfer, V. Bouchiat, T. Ondarçuhu, and M. Monthieux, Nature Nanotechnology **1**, 53 (2006); P. Jarillo-Herrero, J. A. van Dam, and L. P. Kouwenhoven, Nature **439**, 953 (2006); H. I. Jørgensen, K. Grove-Rasmussen, T. Novotný, K. Flensberg, and P. E. Lindelof, Phys. Rev. Lett. **96**, 207003 (2006).
- ² J.A. van Dam, Y.V. Nazarov, E.P.A.M. Bakkers, S. De Franceschi, and L.P. Kouwenhoven, Nature **442**, 667 (2006); T. Sand-Jespersen, J. Paaske, B. M. Andersen, K. Grove-Rasmussen, H. I. Jørgensen, M. Aagesen, C. Sørensen, P. E. Lindelof, K. Flensberg, and J. Nygård, Phys. Rev. Lett. **99**, 126603 (2007).
- ³ C. Buizert, A. Oiwa, K. Shibata, K. Hirakawa, and S. Tarucha, Phys. Rev. Lett. **99**, 136806 (2007).
- ⁴ R. Fazio and R. Raimondi, Phys. Rev. Lett. **80**, 2913 (1998); Phys. Rev. Lett. **82**, 4950 (1999).
- ⁵ K. Kang, Phys. Rev. B **58**, 9641 (1998).
- ⁶ P. Schwab and R. Raimondi, Phys. Rev. B **59**, 1637 (1999).
- ⁷ A. A. Clerk, V. Ambegaokar, and S. Hershfield, Phys. Rev. B **61**, 3555 (2000).
- ⁸ S. Shapira, E. H. Linfield, C. J. Lambert, R. Seviour, A. F. Volkov, and A. V. Zaitsev, Phys. Rev. Lett. **84**, 159 (2000).
- ⁹ J. C. Cuevas, A. Levy Yeyati, and A. Martín-Rodero, Phys. Rev. B **63**, 094515 (2001).
- ¹⁰ C. W. J. Beenakker and H. van Houten, in *Single-Electron Tunneling and Mesoscopic Devices*, edited by H. Koch and H. Lübbig, Springer, Berlin, 1992, pp. 175-179.
- ¹¹ L. I. Glazman and K. A. Matveev, JETP Lett. **49**, 659 (1989).
- ¹² B. I. Spivak and S. A. Kivelson, Phys. Rev. B **43**, 3740 (1991).
- ¹³ A.V. Rozhkov, D.P. Arovas, and F. Guinea, Phys. Rev. B **64**, 233301 (2001).
- ¹⁴ A. A. Clerk and V. Ambegaokar, Phys. Rev. B **61**, 9109 (2000).
- ¹⁵ Y. Avishai, A. Golub, and A.D. Zaikin, Phys. Rev. B **67**, 041301(R) (2003).
- ¹⁶ G. Sellier, T. Kopp, J. Kroha, and Y. S. Barash, Phys. Rev. B **72**, 174502 (2005).
- ¹⁷ R. López, Mahn-Soo Choi, and R. Aguado, Phys. Rev. B **75**, 045132 (2007).
- ¹⁸ F. S. Bergeret, A. Levy Yeyati, and A. Martín-Rodero, Phys. Rev. B **74**, 132505 (2006).
- ¹⁹ C. Karrasch, A. Oguri, and V. Meden, Phys. Rev. B **77**, 024517 (2008).
- ²⁰ Z. Nussinov, A. Shnirman, D. P. Arovas, A. V. Balatsky, and J. X. Zhu, Phys. Rev. B **71**, 214520 (2005).
- ²¹ A. Levy Yeyati, J. C. Cuevas, A. López-Dávalos, and A. Martín-Rodero, Phys. Rev. B **55**, R6137 (1997).
- ²² G. Johansson, E. N. Bratus, V. S. Shumeiko, and G. Wendin, Phys. Rev. B **60**, 1382 (1999).
- ²³ I. A. Sadovskyy, G. B. Lesovik, and G. Blatter, Phys. Rev. B **75**, 195334 (2007).
- ²⁴ S. Ishizaka, J. Sone, and T. Ando, Phys. Rev. B **52**, 8358 (1995).
- ²⁵ Mahn-Soo Choi, Minchul Lee, K. Kang, and W. Belzig, Phys. Rev. B **70**, 020502(R) (2004).
- ²⁶ F. Siano and R. Egger, Phys. Rev. Lett. **93**, 047002 (2004).
- ²⁷ E. Vecino, A. Martín-Rodero, and A. Levy Yeyati, Phys. Rev. B **68**, 035105 (2003).
- ²⁸ Mahn-Soo Choi, C. Bruder and D. Loss, Phys. Rev. B **62**, 13569 (2000).
- ²⁹ M.G. Pala, M. Governale, and J. König, New J. Phys. **9**, 278 (2007).
- ³⁰ A. F. Volkov, Phys. Rev. Lett. **74**, 4730 (1995); F.K. Wilhelm, G. Schön, and A.D. Zaikin, Phys. Rev. Lett. **81**, 1682 (1998); S.-K. Yip, Phys. Rev. B **58**, 5803 (1998); P. Samuelsson, J. Lantz, V. S. Shumeiko, and G. Wendin, Phys. Rev. B **62**, 1319 (2000); E. V. Bezuglyi, V. S. Shumeiko, and G. Wendin, Phys. Rev. B **68**, 134506 (2003); F. Giazotto, T.T. Heikkilä, F. Taddei, R. Fazio, J.P. Pekola, and F. Beltram, Phys. Rev. Lett. **92**, 137001 (2004).
- ³¹ J.J.A. Baselmans, A.F. Morpurgo, B.J. van Wees, T.M. Klapwijk, Nature **397**, 43 (1999).
- ³² J. Bardeen, Phys. Rev. Lett. **9**, 147 (1962); B.D. Josephson, Phys. Lett. **1**, 251 (1962).
- ³³ Y. Meir and N.S. Wingreen, Phys. Rev. Lett. **68**, 2512 (1992).
- ³⁴ J. König, H. Schoeller, and G. Schön, Phys. Rev. Lett. **76**, 1715 (1996); J. König, J. Schmid, H. Schoeller, and G. Schön, Phys. Rev. B **54** 16820 (1996).
- ³⁵ In the case of a normal line, the factor $|\Delta/\omega|$ is not present, but the argument remains the same.